Hybrid Dendritic Molecules with Confined Chromophore Architecture to Tune Fluorescence Efficiency

Pascal André,*,†,§ Ge Cheng,‡,§ Arvydas Ruseckas,†,§ Tanja van Mourik,‡ Herbert Früchtl,‡ Joe A. Crayston,‡,§ Russell E. Morris,‡ David Cole-Hamilton,*,‡,§ and Ifor D. W. Samuel*,†,§

SUPA, School of Physics and Astronomy, University of St. Andrews, St. Andrews, Fife, UK KY16 9SS; EaStCHEM, School of Chemistry, University of St. Andrews, St. Andrews, Fife, UK KY16 9ST; and Organic Semiconductor Centre, University of St. Andrews, St. Andrews, Fife, UK KY16 9SS

Received: July 4, 2008; Revised Manuscript Received: October 11, 2008

The aim of this publication is to present a general strategy to engineer more efficient photoluminescent dendritic molecules based on polyhedral oligomeric silsesquioxane (POSS) cores. A series of chromophores were grafted on POSS cores to form dendritic molecules for which steric hindrance was used as a trigger to tune their photophysical properties. For fluorescence in the blue/near-UV spectral ranges, 4-vinylbiphenyl molecules were chosen as model chromophores to present a general approach based on stable chemistry and bulky groups grafted to the chromophores to enhance photoluminescence efficiency of the dendritic molecules. Photoluminescence quantum yields as well as steady-state and time-resolved solution spectroscopy along with molecular dynamics investigation and electronic structure calculations on a family of new materials are reported. We highlight an apparent contrast between free chromophore and dendritic molecules photophysical properties and show that chromophores' engineering and confinement around an inorganic core allows the design of more efficient photoluminescent dendritic molecules relevant to sensors and hybrid light-emitting diodes.

I. Introduction

Dendrimers have recently received considerable attention as specific properties are expected to arise from their highly branched and symmetric architecture. In addition to the development of different synthetic approaches which lead to ever more complex dendrimers,[1−4] various applications are currently under investigation which include catalysis,[5−8] encapsulation and drug delivery,[4,9−11] nano/ultrafiltration and phase transfer,[12,13] as well as nanomaterial preparation.[14,15]

Over the past few years, dendritic molecules have also been successfully designed to create a new class of materials for organic light-harvesting systems as well as light-emitting diodes and photoactive devices.[4,16−27] For instance, successful syntheses and characterizations of a few red, green, and blue emitting dendritic molecules have recently been reported in the literature,[24−27] using independent alterations of the core, the branches (dendrons), and the external surface groups. This has been shown to allow tuning of the emission spectra as well as favoring energy transfer between the core and the periphery.[22,28] Another advantage of this strategy is that it prevents both dye molecule aggregation[27−30] and excimer formation,[18,23,31,32] while preserving simple solution processing for future applications. Other dendrimer architectures with, for instance, chromophores located both on the dendrons and in the core have also been extensively investigated, revealing, for instance, intramolecular energy and electron transfer[33−40] along with intramolecular interactions leading to excimer formation and either enhancement or quenching of the photoluminescence, depending upon the system under investigation.[41−43]

To control the material properties, different architectures can be considered and inorganic symmetric building blocks can be used as a core around which dendrons with specific chromophores can be grafted. The polyhedral oligomeric silsesquioxane (POSS) with eight silicon corners proves to be an appropriate model compound, which has indeed been extensively studied and has been found to display versatile chemistry.[44−46] Furthermore, it has attracted interest for a few potential applications,[7,47,48] including in the organic semiconductor field when it was grafted onto the end of conjugated polymers, improving thermal stability and providing higher brightness and photoluminescence efficiency attributed to the reduction of defects and/or aggregation of the conjugated polymer.[49] Similarly, higher photoluminescence efficiency was reported for polyfluorenes grown at the eight corners of the silicon oxide cube,[50] and chromophore-substituted octavinylsilsesquioxane has started to be developed for OLED applications.[51−54]

Numerical simulations of various levels of theory can be used to determine electronic properties[55−57] and to gain insight into molecular conformations. In the context of dendritic molecules, hydrodynamic radii, extension and back-folding, crowding, and dendron flexibility have been investigated as a function of dendrimer generation and solvent quality.[58−62] Assemblies of nanostructured POSS networks have been studied by lattice Monte Carlo simulations in order to explore the effect of linker length on porosity and spatial distributions of the building blocks in 3D structures.[63] The crystalline structure and electronic properties of single POSS core derivatives have been studied by numerical simulations and compared with experimental results, providing increased insight into the properties of single hybrid organic−inorganic nanomaterials.[45,48]

* Corresponding authors. E-mail: Pascal.Andre@st-andrews.ac.uk, djc@st-and.ac.uk, idws@st-and.ac.uk.
† SUPA, School of Physics and Astronomy.
§ Organic Semiconductor Centre.
‡ EaStCHEM, School of Chemistry.

10.1021/jp806031q CCC: $40.75
Published on Web 12/04/2008

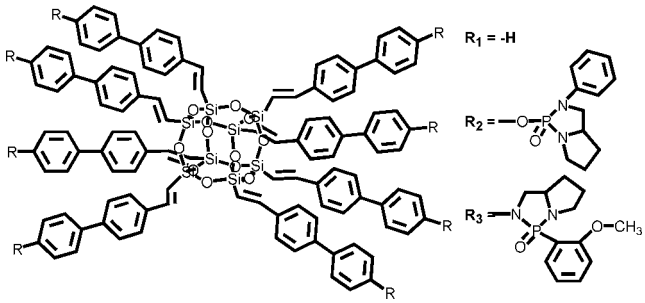

Figure 1. Dendritic molecules based on silsesquioxane core with various functionalized chromophores: vbp (R_1), vbp-O (R_2), and vbp-N (R_3).

Motivated by the potentials of hybrid organic−inorganic materials, the present publication reports on the design, synthesis, modeling, and photophysical properties of three dendritic molecules. 4-Vinylbiphenyl (vbp, Figure 1) was used as the initial chromophore, and two other chromophores with different bulky groups attached at the 10-position of the vinyl biphenyl group were synthesized (vbp-O and vbp-N, Figure 1). A convergent synthetic approach was implemented to make organic−inorganic hybrid photoluminescent dendritic molecules, all based on the same silsesquioxane core and vinylbiphenyl.

The photophysical properties were investigated both by steady-state and time-resolved spectroscopy. To gain insight into the conformations of the dendritic molecules and to explain features of the photophysical properties of the materials, force field molecular dynamics and electronic structure calculations were completed; see Supporting Information for details. Major differences in behavior between the three different dendritic molecules were indeed observed, including absorbance and photoluminescence (PL) shifts as well as variation of PL efficiencies and lifetimes. The progressive enhancement of the PL efficiency shown by the POSS-derivative family is explained by the confinement of the chromophores around the POSS core, by the structure of the peripheral groups, and by the nature of the chemical bridge linking the chromophore and the peripheral groups. Our work demonstrates the flexibility of such hybrid dendritic molecules to tune the photophysical properties of luminescent materials.

II. Experimental Section

II.1. Materials, Synthesis, and Characterization. Solvents and 4-vinylbiphenyl were purchased from Sigma-Aldrich, distilled when indicated and used without further treatment otherwise.

The 4-vinylbiphenyl chromophore was chosen for its ability to be chemically modified, its relatively high photoluminescence quantum yield (PLQY, ≈0.61 in cyclohexane), and its weak oxygen quenching (by ≈15% of the measured value), allowing straightforward investigations.[64] In addition, from a chemical point of view, this building block offers the opportunity both to be easily linked to the silsesquioxane and to design branches with different steric hindrance which is the main trigger investigated in this study.

The additional bulky groups have been chosen in order to induce some interaction such as hydrogen bonds and steric and/or aromatic interactions[65] without, however, inducing any large increase of the conjugation length of the 4-vinylbiphenyl, so that they offer the opportunity to compare chromophores having similar photophysical characteristics.

The chromophores were attached to a POSS core by cross-metathesis of octavinylsilsesquioxane catalyzed by Grubbs' catalyst. The product was then extracted in order to remove any byproduct and characterized by both nuclear magnetic resonance (NMR) and matrix-assisted laser desorption/ionization (MALDI) mass spectra. The details of the syntheses and characterizations will be reported separately.[66]

II.2. Apparatus and Data Treatment. Absorption and photoluminescence properties of the chromophores and dendritic molecules were investigated at room temperature in optically dilute solutions. Solvents were not degassed. Dichloromethane, CH_2Cl_2, was the main solvent used in this work. A few other solvents such as tetrahydrofuran, chloroform, and cyclohexane were also used to assess the consistency of the results. No significant differences between the results obtained with different solvents were observed, and so, for the sake of clarity, all the results shown here are for CH_2Cl_2 as a solvent.

II.2.1. Absorption-PL-PLE. Absorption spectra were recorded using a Cary 300 spectrophotometer and 10 mm optical path fluorescence cuvettes (Hellma), and the concentration was adjusted to reach an optical density of about 0.1, leading to a molar concentration of about 3.2×10^{-6}, 2.6×10^{-6}, and 2.9×10^{-6} M for the chromophores and 0.3×10^{-6}, 0.3×10^{-6}, and 0.5×10^{-6} M for the dendritic molecules based on vbp, vbp-O, and vbp-N, respectively.

Photoluminescence (PL) and photoluminescence excitation (PLE, not presented) spectra were recorded with a Jobin Yvon Horiba Fluoromax 2 fluorimeter. Spectra were corrected for grating and detector sensitivity variation with wavelength. Absorption and PL spectra were fitted with Gaussians, which were used to provide the peak values reported herein.

The solution photoluminescence quantum yields (PLQY) were measured using quinine sulfate (Fluka) in 0.5 M sulfuric acid (Sigma-Aldrich) solution as a standard because of its known quantum yield of 54.6% as well as its very small sensitivity to oxygen quenching.[67] The following equation was used to perform the appropriate corrections:[67]

$$\Phi_x = \Phi_r\left(\frac{A_r(\lambda_r)}{A_x(\lambda_x)}\right)\left(\frac{I(\lambda_r)}{I(\lambda_x)}\right)\left(\frac{n_x}{n_r}\right)^2\left(\frac{D_x}{D_r}\right) \quad (1)$$

where Φ stands for PLQY and the subscripts x and r refer to the compound to be characterized and to the reference solutions, respectively. λ is the excitation wavelength, $A(\lambda)$ is the absorbance, $I(\lambda)$ is the relative intensity of the exciting light, n is the solvent refractive index, and D is the integrated area under the corrected emission spectra.

II.2.2. Time-Resolved Spectroscopy. Time-resolved fluorescence (TRF) measurements were carried out using an optical parametric amplifier pumped by an amplified Ti:sapphire femtosecond laser system operating at a pulse repetition rate of 5 kHz and a synchro-scan streak camera with a time resolution of ∼3 ps. The pulse duration was 100 fs, and the excitation wavelengths were 266 and 295 nm (4.66 and 4.20 eV, respectively).

The photoluminescence decays were fitted by a single- or double-exponential model using a nonlinear least-squares procedure:[68]

$$I(t) = \sum \alpha_i \exp(-t/\tau_{PLi}) \quad (2)$$

where $I(t)$ is the photoluminescence intensity as a function of time, τ_{PL} is the PL decay time, and α is the pre-exponential factor associated with each decay time. α represents the

amplitude of the components at $t = 0$ and $\sum\alpha_i$ are normalized to unity. In case of a double-exponential decay, the lifetime weighted quantum yield, also called average lifetime, is defined as[68]

$$\alpha_{avg} = \sum \alpha_i \tau_{PLi} \quad (3)$$

II.3. Cyclic Voltammetry. Cyclic voltammetry was recorded in 0.1 M $TBAPF_6$ in DMF at a voltage scan rate of 100 mV/s. All the compounds were sufficiently soluble in DMF; in addition, the monomers only were sufficiently soluble in acetonitrile. The reduction potentials were quite negative, so care had to be taken to ensure that the background current response was minimal. Best results were obtained using a glassy carbon electrode (3 mm diameter) in freshly vacuum-distilled DMF. The reductions were also associated with precipitation onto the electrode so the electrode had to be frequently repolished. A platinum wire counter electrode was used with a silver/(0.1 M $AgNO_3$ MeCN) reference electrode. Potentials were then adjusted to the ferrocene potential after addition of ferrocene as an internal standard. An EG&G PAR 270A potentiostat was used with M270 software.

The data analysis was completed as follows:[69,70]

$$\text{HOMO (eV)} = -\text{IP} = -(E_{onset}(\text{oxidation}) + 4.8) \quad (4)$$

$$\text{LUMO (eV)} = -\text{EA} = -(E_{onset}(\text{reduction}) + 4.8) \quad (5)$$

$$E_g^{elec}\,(\text{eV}) = \text{LUMO} - \text{HOMO} \quad (6)$$

where HOMO is the highest occupied molecular orbital, IP is the ionization potential, E_{onset} is the potential at which the current starts to rise and is defined as the potential to achieve about 5% of the peak current, LUMO is the lowest unoccupied molecular orbital, EA is the electron affinity, 4.8 eV is the ionization energy of ferrocene, and E_g^{elec} is the electrochemical band gap.

II.4. Modeling. ***II.4.1. Electronic Structure Calculations.*** The structure of 4-vinylbiphenyl was optimized with DFT using the B3LYP functional[71] and second-order Møller−Plesset perturbation theory (MP2), using the 6-31+G(d) basis set. For both methods rotational energy profiles were calculated by optimizing the structure at fixed values of the torsion angle between the two aromatic rings (defined by four consecutive carbon atoms including the two carbon atoms linking the phenyl rings and their immediate neighbors).

In the B3LYP structures the vinyl group was found to be coplanar with the adjacent phenyl ring. In the MP2-optimized structures the vinyl group is twisted out of the phenyl plane by ~30°, and considering the symmetry of the vinylbiphenyl molecule all excitation energies were calculated for torsion angles between 0° and 90°.

At each geometry the vertical excitation energy was computed using TD-DFT[72] at the B3LYP level, CIS(D),[73,74] and ZINDO/S.[75] The TD-DFT and CIS(D) calculations employed the 6-31+G(d) basis set. The ZINDO/S calculations were done with ORCA.[76] All other calculations employed the Gaussian program package.[77]

ZINDO/S was also used to simulate excitation spectra of the branch molecules and the complete dendritic molecules. The geometries of both the isolated molecules and the dendritic molecules were first annealed and then optimized using the AMBER force field in Hyperchem. The ZINDO/S absorption energies and oscillator strengths were subsequently computed using ORCA. The utility program orca_mapspc (part of the ORCA distribution) was used to calculate simulated spectra from those values. The transition peaks were approximated by Gaussian functions with a full width at half-maximum of 1000 cm^{-1}, corresponding to a wavelength of 10 nm. We also compared the spectra of the branch molecules where the terminating hydrogen was replaced by an SiH_3 group to separate the effect of geometry change in the dendritic molecules compared to the free branch from the effect of delocalization induced by the POSS core.

II.4.2. Molecular Dynamics. The geometries of the dendritic molecules were built using Hyperchem.[78] All the relevant atoms were labeled in order to prepare the data analysis. After having optimized the structure of each dendritic molecule, molecular dynamics was used to determine the average conformations. For comparison purposes, MM+ and AMBER were used alternatively as force fields and led to similar results.

For every simulation, energies, temperatures, and atom coordinates were monitored to allow the analysis of the trajectories. Atomic coordinates of the dendritic molecules were extracted from the snapshot files and used to calculate distances and angles over more than 1500 frames. These were subsequently averaged and analyzed to produce frequency histograms of parameters such as radii of gyration, moments of inertia, distances between atoms, backfolding, and torsion angles; see the Supporting Information for details.[76]

III. Results

III.1. Photophysical Characterization. The photophysical properties of the three free chromophores measured in CH_2Cl_2 at room temperature are shown in Figure 2 and summarized in Table 1.

Consistent with the literature, the vbp chromophore shows an absorption peak at ~278 nm.[64] When compared with vbp, the absorption peaks of the other chromophores are slightly red-shifted: a few nanometers in the case of the vbp-O chromophore with an oxygen bridge and a larger red shift of about 26 nm in the case of the vbp-N chromophore designed with a nitrogen bridge (see Table 1 and Figure 2A−C (solid symbols)). The fluorescence spectrum of the vbp chromophore shows a substructure in the UV range with a full width at half-maximum of 52 nm. The bulkier chromophores led to a weakening of the substructure, a red shift of the peaks (vbp-O ~ 10 nm, vbp-*N* > 40 nm), a broadening, a tailing toward larger wavelengths of the fluorescence spectra, and a larger spectral shift between the absorbance and the fluorescence peaks. As an illustration, the photoluminescence full width at half-maximum, δ_{PL}, of vbp-N is about 15 nm larger than those measured with the two other free chromophores, and the full width at 10% of the maximum of the fluorescence curves, δ_{PL10}, continuously increases from 88 to 149 nm (see Table 1). A detailed analysis of the PL spectra based on five Gaussian transitions of equal width is presented in the Supporting Information.

The 45% solution PLQY of the 4-vinylbiphenyl chromophore (see Table 1) is consistent with the value reported in the literature, considering that the present measurements were performed in ambient atmosphere containing oxygen.[64] When bulkier groups were connected to the chromophore, the PLQY decreased to 10% for vbp-N.

Time-resolved fluorescence measurements were then performed to further investigate the chromophore relaxation

TABLE 1: Absorbance Peak, Position of the First Photoluminescence Peaks and Associated Spectral Shift between the Absorbance and PL Peaks, Fluorescence Full Width at Half-Maximum (δ_{PL}) and at 10% Maximum (δ_{PL10}), Photoluminescence Quantum Yield (PLQY) Measured at the Absorbance Maximum, Photoluminescence Decay and Associated Amplitude of the Fit (τ_{PL}, α), Average Decay (τ_{av}) Obtained with 295 nm as the Excitation Wavelength (See *Supporting Information* for Details)[76]

	vbp	vbp-O	vbp-N	POSS-vbp	POSS-vbp-O	POSS-vbp-N
abs peak (nm)	278	281	304	287	290	316
1st PL peak (nm)	317	325	360	330	342	387
abs-PL shift (nm)	39	44	55	43	52	73
δ_{PL}, δ_{PL10} (nm)	52, 88	52, 99	67, 149	60, 123	62, 130	81, 156
PLQY (%)	45	38	10	≤4	14	58
τ_{PL} (ns), α	1.58, 1.00	0.13, 0.45 2.39, 0.55	0.11, 0.69 0.33, 0.31	0.03, 1.00	0.09, 0.78 1.32, 0.22	0.31, 0.22 1.53, 0.78
τ_{avg} (ns)	1.58	1.37	0.19	0.03	0.35	1.24

processes (see Table 1 and Figure 2D−F (solid symbols)). The 4-vinylbiphenyl is characterized by a single exponential photoluminescence decay. The measured photoluminescence lifetime, τ_{PL} (1.58 ns), was found to be consistent with the natural lifetime reported in the literature (1.30 ns),[64] considering that they were obtained in two different solvents, dichloromethane and cyclohexane, respectively. However, when an additional bulky group is grafted, the photoluminescence decay is much faster and presents a multiexponential behavior which indicates heterogeneity. This is consistent with a larger range of conformations of the chromophore as a result of the additional bulky groups. By increasing the size of the bulky group connected to the 4-vinylbiphenyl, the amplitude, α, of the fast decay component increases (see Table 1).

Once grafted to the silsesquioxane core to form the dendritic molecules, both the absorbance and photoluminescence spectra of the chromophores present slight feature variations (see Figure 2). Compared to the free chromophores, the photophysical properties of the corresponding dendritic molecules mainly differ in the following aspects: (a) the absorbance and photoluminescence peaks show a bathochromic shift, (b) the structure of the fluorescence of the dendritic molecule is weakened and the transitions present a larger energy width,[64] (c) the spectral shift between the absorbance and PL peaks is larger, and (d) the photoluminescence spectra are broader (larger full width at half-maximum, δ_{PL}, as well as a longer tailing, as shown by the larger $\delta_{PL10\ value}$).

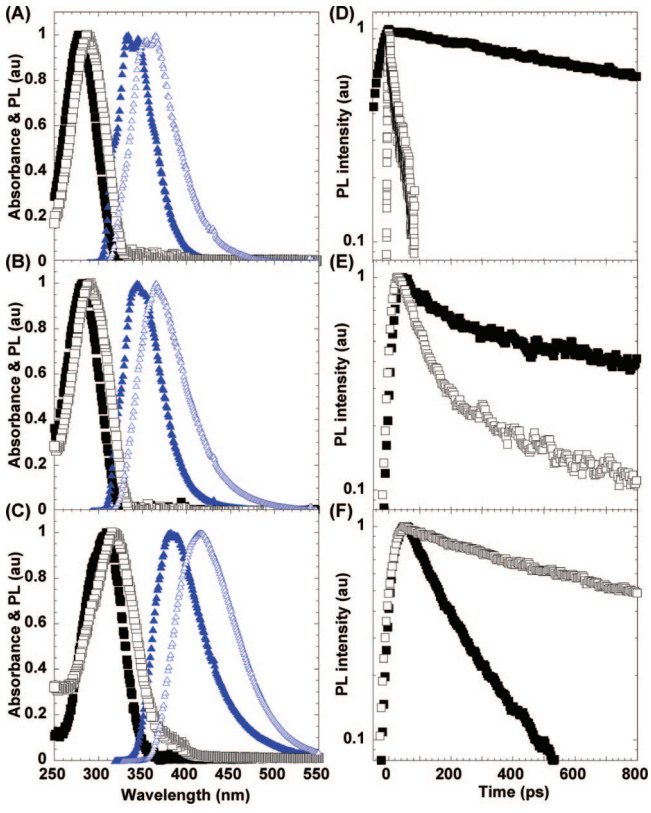

Figure 2. Normalized absorption (■) and photoluminescence (▲) spectra (A, B, C) associated with their time-resolved fluorescence (D, E, F) with 295 nm as the excitation wavelength. (A, D), (B, E), and (C, F) correspond to compounds based on vbp, vbp-O, and vbp-N, respectively, as illustrated in Figure 1. Solutions of free chromophores (solid symbols) and dendritic molecules (open symbols) are shown. Measurements were completed at room temperature.

When POSS-vbp derivatives are compared with each other, it appears that the photoluminescence quantum yield of the dendritic molecules increased with the size of the grafted bulky groups, whereas it decreased for the free chromophores (see Table 1). Starting from 4% with POSS-vbp, the PLQY increased when bulkier groups were connected to the chromophore, reaching 14% and 58% for POSS-vbp-O and POSS-vbp-N, respectively.

Figure 2D−F (open symbols) presents data associated with time-resolved fluorescence, which was investigated to get more insight into the relaxation processes. Deduced lifetimes are provided in Table 1. The dendritic molecule POSS-vbp, having the smallest branches, shows very fast decay of photoluminescence, τ_{PL}, which is more than 10 times faster than those associated with the free vbp chromophores (see Figure 2D). Within the experimental uncertainty and for these two compounds, a similar PLQY decrease is observed.

For the dendritic molecule POSS-vbp-O, the time-resolved fluorescence is characterized by a multiexponential decay, as in the case of the free vbp-O chromophore (see Figure 2E). In this case, the fast and slow components associated with the photoluminescence lifetimes, τ_{PL}, have the same order of magnitude in the grafted and free chromophores (1.32 vs 2.39 ns and 0.09 vs 0.13 ns). The amplitude, α, associated with the fast decay of the dendritic molecule POSS-vbp-O becomes the largest fraction while the average lifetime, τ_{avg}, and PLQY are reduced by a similar factor of about 3.5.

In the case of the dendritic molecule POSS-vbp-N, with the bulkiest group, the time-resolved fluorescence measurement shows also a multiexponential behavior as observed with the free chromophores (see Table 1). τ_{PL} of the dendritic molecule POSS-vbp-N are both slower than the parameters fitted from the spectra of the free chromophores (0.31 vs 0.11 ns and 1.53 vs 0.33 ns). The amplitude, α, of the slowest decay becomes larger in the case of the dendritic molecule POSS-vbp-N than with the free vbp-N chromophore (0.31 vs 0.78). Average lifetime, τ_{avg}, and PLQY are both increased by a similar factor of about 6.

More striking may be the comparison of Figure 2D−F. Indeed, the decay curves associated with the time-resolved

TABLE 2: Electrochemical Data for Chromophores Derivatives Obtained by Cyclic Voltammetry[a]

	vbp	vbp-O	vbp-N	POSS-vbp	POSS-vbp-O	POSS-vbp-N
E_p^{anodic} (V vs f)	+1.058	+1.115	+0.750	+0.813	+0.895	+0.810
E_{onset} (V vs f)	+0.85	+0.90	+0.65	+0.75	+0.80	+0.63
HOMO (eV)	−5.65	−5.70	−5.45	−5.55	−5.60	−5.43
$E_p^{cathodic\ 1}$ (V vs f)	−2.814	−2.792	−2.826	−2.886	−2.854	−2.877
$E_p^{cathodic\ 2}$ (V vs f)	−3.212	−3.076	−3.226	−3.262	−3.120	−3.215
E_{onset} (V vs f)	−2.56	−2.43	−2.56	−2.43[b]	−2.38[b]	−2.67[b]
LUMO (eV)	−2.24	−2.37	−2.24	−2.37	−2.42	−2.13
E_g^{elec} (eV)	+3.41	+3.33	+3.21	+3.18	+3.18	+3.30

[a] E_p^{anodic} is the potential associated with an anodic (i.e., oxidation) voltage peak in volts vs ferrocene, setting the zero of the voltage scale to be the ferrocene level, $E_p^{cathodic}$ is the potential associated with a cathodic (i.e., reduction) voltage peak, E_{onset} is the onset potential, and E_g^{elec} (eV) is the electrochemical band gap. In DMF/0.1 M $TBAPF_6$; scan rate 100 mV s^{-1}. Peak potentials ±5 mV; onsets ±10 mV; E_g^{elec}(eV) with uncertainty ±0.02 eV. [b] Onset of reduction broader than the monomers.

luminescence of the free vbp chromophore stands above the curve associated with the POSS-vbp which decays much faster (see Figure 2D). This behavior is still observed in the case of the vbp-O derivatives (see Figure 2E), even though it should be noticed that the variation of the decay curves between free dendrons and dendritic molecules seems somehow dampened compared to vbp derivatives. What is, however, striking and, at first sight, surprising in the case of the vbp-N derivatives (see Figure 2F) is that the opposite behavior is observed. Indeed, the decay curves associated with the dendritic molecule stands above the free dendrons which this time is the compound showing the fastest photoluminescence decay. Consequently, it is clear that the free dendrons, solid symbols, decay faster with the grafted bulky groups, whereas the dendritic molecules, open symbols, show a progressive slower decay as the dendrons have been engineered with bulkier groups. The reasons for this opposite behavior between free dendrons and dendritic molecules are discussed in the following section.

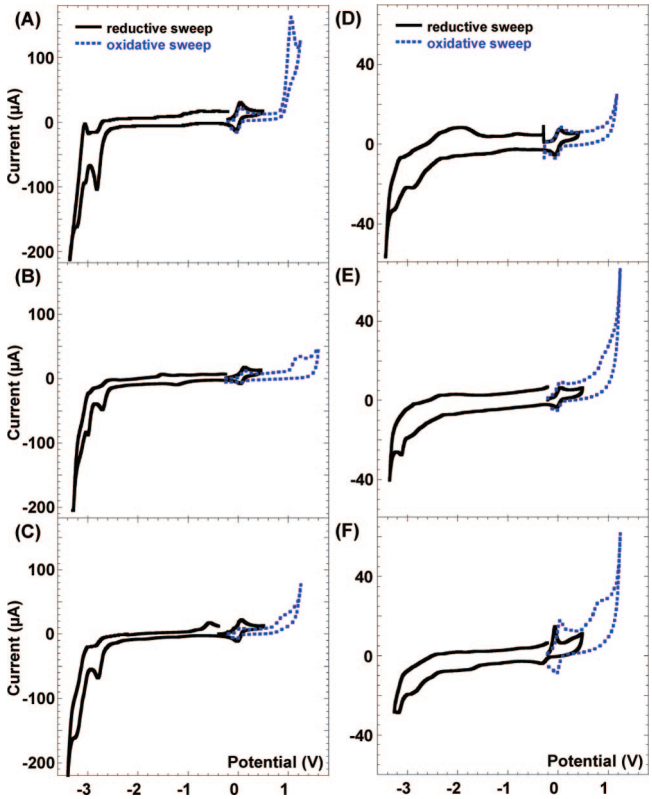

Figure 3. Cyclic voltammetry scans in DMF/0.1 M $TBAPF_6$; scan rate 100 mV s^{-1}. Thick (dark) curve is the cathodic (reductive) sweep, and the dotted (blue) curve is the anodic (oxidative) sweep.

III.2. Cyclic Voltammetry. All the experimental data obtained by cyclic voltammetry are presented in Figure 3 and summarized in Table 2.

The model compound, vbp, showed an irreversible one-electron reduction in both DMF and acetonitrile. This was followed closely by a further reduction (preceded by a smaller adsorption or solution wave) which showed signs of an anodic peak. It is possible that this second reduction is due to a product of the first, since it is preceded by an irreversible process and its relative height varied with scan rate.

The vbp compound was also irreversibly oxidized by between 1 and 2 electrons, again suggesting that the product is itself electroactive. The vbp-O and vbp-N derivatives showed similar features and similar redox potentials, with the greatest difference being exhibited by the easier oxidation of vbp-N, whose oxidation was cathodically shifted by about 250 mV compared to vbp.

It can be noticed that the electrochemical band gap of the free chromophores follow the same trend as the optical band gap (see Tables 1 and 2) with

$$E_g(\text{vbp}) > E_g(\text{vbp-O}) > E_g(\text{vbp-N})$$

In this context the electrochemical data complement nicely the photophysical investigation completed on the free chromophore and highlight the slight variation of the HOMO and LUMO levels induced by the grafted bulky groups.

When attached to the POSS core the vbp exhibited the same features at similar potentials, indicating that the vinyl groups were intact, but the peaks were much broader and the limited solubility in DMF led to peaks which were small compared to the background current of the carbon electrode. The electrochemistry of the POSS derivative was complicated by electrode fouling after scanning over the reductions leading occasionally to broad product adsorbate peaks at about −1.5 to −2.5 V. In this context it can be noticed that (see Tables 1 and 2)

$$E_g^{elec}(\text{POSS-vbp}) = E_g^{elec}(\text{POSS-vbp-O}) < E_g^{elec}(\text{POSS-vbp-N})$$

whereas optically a strongly different variation was observed

$$E_g^{opt}(\text{POSS-vbp}) > E_g^{opt}(\text{POSS-vbp-O}) > E_g^{opt}(\text{POSS-vbp-N})$$

This apparent discrepancy is likely to be due to more dilute solutions imposed by the lower solubility in DMF of the dendritic molecules compared to their associated free chromophore (see scales of the current in Figure 3A−C vs Figure 3D−F) which leads to greater broadness and weakness of the POSS electrochemical peaks and the consequent uncertainties in the "onsets" determination.

IV. Discussion

For all materials, the absorption and PL measurements were found to be independent of the irradiation time so that degradation or photochemical reaction of the dendritic molecule could be excluded. The photophysical properties of the dendritic molecules were found to be independent of both the solvent (CH_2Cl_2, $CHCl_3$, tetrahydrofuran) and the concentration over a factor 10, thus ruling out intermolecular aggregates. The presence of impurities and byproduct was excluded since the three dendritic molecules were analytically pure and mass spectroscopic studies showed single peaks corresponding to a single molecular weight of 1851, 3740, and 3853 Da, consistent with a full substitution at each corner of the POSS core for each dendritic molecule (POSS-vbp, POSS-vbp-O, and POSS-vbp-N, respectively).

The main features of the photophysical properties are (i) a slight bathochromic shift and sharp decrease of the PL efficiency when bulky groups are grafted to a free vbp unit and (ii) a slight bathochromic shift and large variation of the PL efficiency when the dendron is attached to the POSS core. However, to develop a general strategy to engineer more efficient photoluminescent dendritic molecules, what needs to be explained is why the free chromophore having the lowest PL efficiency leads to the POSS derivative showing the highest PL efficiency, and vice versa.

IV.1. Bathochromic Shift. As illustrated in Figure 2A, the photophysical properties of the vinylbiphenyl molecule are in good agreement with the data reported in the literature (λ_{ex} = 278 nm, PLQY = 0.45, in air).[64] In the cases of vbp-O and vbp-N, the addition of a bulky group to the vinyl biphenyl had very little effect on the absorbance and PL properties. The spectra are only slightly broadened and show very small bathochromic shifts (see Table 1 as well as Figure 2A−C). These shifts could be explained by a larger delocalization of the electrons, resulting from the free electron pair associated with oxygen and nitrogen along with their electron-donating ability (Pauling electronegativity: C 2.55, N 3.04, O 3.44)[79] and the more rigid nitrogen bridge. To address this element more rigorously, the absorption spectra were simulated, and the normalized ZINDO/S calculations are presented in Figure 4.

The spectra show the calculated absorption peaks convoluted with Gaussians centered on the peaks and having full width at half-maximum of 10 nm. This "band" representation has been chosen to provide an easier comparison with the trends observed experimentally. As illustrated in Figure 4, ZINDO/S calculations of vbp, vbp-O, and vbp-N show one absorption peak in the spectral region of interest. As expected, only qualitative agreement was obtained between the experimental and simulated data. The calculations slightly underestimate the band gap energy of the chromophores but reproduce correctly the slight red shift of the series vbp, vbp-O, and vbp-N, as discussed later in the text.

When the vbp derivatives were grafted to the POSS core, a red shift of both the absorbance and the PL peaks together with a broadening of the PL spectrum resulted (see Figure 2).

Potential explanations, explored in the following sections, include: (a) Confinement around the POSS core: Conformational and environmental effects on the chromophores. (b) Potential electron delocalization onto the POSS core. In addition, the low-energy peaks displayed by the calculation are discussed later in the text as well as in the Supporting Information.

IV.1.1. Conformation (Electronic Structure and Molecular Dynamics). The equilibrium torsion angle between the two phenyl rings in vbp is a compromise between the effect of the conjugation of the π electrons and the steric repulsion of the ortho-hydrogen atoms. Consequently, the ground state and first excitation energy of a single, isolated vbp was calculated as a function of the torsion angle between the two phenyl rings (see Figure 5).

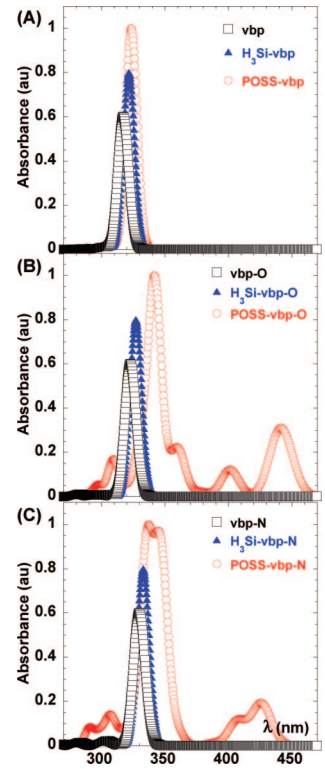

Figure 4. Normalized simulated absorption spectra from the ZINDO/S calculations for the compounds vbp (A), vbp-O (B), and vbp-N (C) derivatives. Free chromophores (□), $-SiH_3$-terminated chromophores (▲), and dendritic molecules (○). All the structures have been annealed and minimized. See text for details.

The MP2 calculations favor noncoplanar structures to a larger extent than the B3LYP calculations, similar to what has been observed in biphenyl.[80] The optimal torsion angle (39° at the B3LYP/6-31+G(d) level; 48° at the MP2/6-31+G(d) level) is in good agreement with the experimental (44.2°)[81] and computed (39−48°)[57,80,82,83] torsion angle in biphenyl. As expected, a red shift is obtained as the torsion angle is decreased (flatter molecule, conjugation length increased), and a blue shift results as the torsion angle is increased (conjugation length decreased).[84] Electronic calculations can however only provide static data,

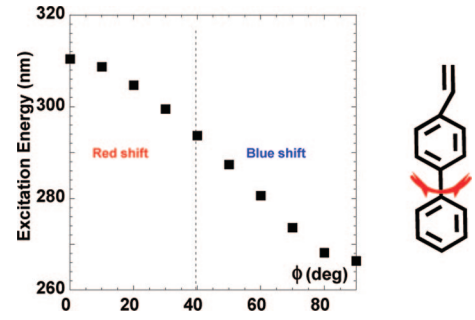

Figure 5. TDDFT excitation energies computed with B3LYP/6-31+G(d) as a function of the torsion angle between the two phenyl rings as illustrated on the right-hand side. The geometries at fixed torsion angle were optimized using B3LYP/6-31+G(d). CIS(D) and ZINDO/S calculations show similar profiles (see SI-Figure 1). The vertical dotted line illustrates the optimal torsion angle of the vbp chromophore at the B3LYP/6-31+G(d) level (39°).

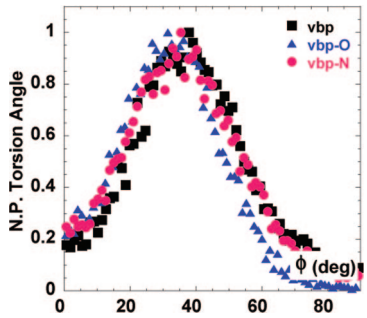

Figure 6. Biphenyl group conformation: torsion angle distribution for the three dendritic molecules obtained by molecular dynamic simulation.

so that further insight into the conformation of the dendritic molecules was sought with molecular dynamics simulations.

Thermal agitation indeed creates a distribution of torsional angles and the normalized populations of the torsion angles between the two adjacent phenyl groups located on the same branch can then be calculated (see Figure 6).

All dendritic molecules studied in this work have a similar torsion angle, with 37.1° (38.8°), 31.9° (36.0°), and 35.0° (40.1°) corresponding to the peak (standard deviation) of the torsion angles associated with POSS-vbp, POSS-vbp-O, and POSS-vbp-N, respectively. The similar values of the torsion angle population for the three materials mean that changes in this angle do not explain the bathochromic shifts observed experimentally between the three dendritic molecules.

IV1.2. Environmental Effects. The confinement of the branches in the vbp-based molecules could result in a local change of the polarizability,[85] as the chromophores will be closer to one another than if they were in solution and not grafted to the POSS core. Molecular dynamics simulations indicate that by grafting bulky groups, the radius of gyration of POSS-vbp increases from 8.8 to 12.4 and 12.9 Å for POSS-vbp-O and POSS-vbp-N, respectively (see Supporting Information for details). The low values of the anisotropy of the moment of inertia indicate fairly spherical molecules in each case, which is consistent with the stiffness of the vinyl bridge connecting the POSS core to the biphenyl derivatives as illustrated by the fairly constant vbp extension (~10.8 Å, see SI-Figure 5D) from the POSS core; see Supporting Information for details.[76] On the other hand, Figure 7 shows the distribution of the Si−C_{19} distances, i.e., beyond the vbp group. Two peaks are observed illustrating two different populations: one containing conformations with C_{19} stretching out of the dendritic molecules and the other adopting backfolded conformations. This is not surprising considering on the one hand the rigidity of the nitrogen "lock" to be compared with the flexibility of the oxygen bridge and on the other hand the slightly bulkier structure of the N-derivative with its extra methyl group. Figure 7 also illustrates that the branches of POSS-vbp-O are much more mobile than the branches of POSS-vbp-N. This could indicate that, once the chromophores of the POSS derivatives have bulky groups grafted to the vbp, their backfolding within the vbp sections of the branches provide access to both more conformations and different environments while contributing to the observed bathochromic shifts and the loss of PL features equivalent to larger energy width of the vibronic transitions. However, if environmental effects were the main contributions, we would expect to observe a larger red shift with POSS-vbp-O than with POSS-vbp-N because of its larger backfolding. The observed values are 9 and 12 nm, respectively (see Table 1), which within the experimental uncertainty does not support this assumption.

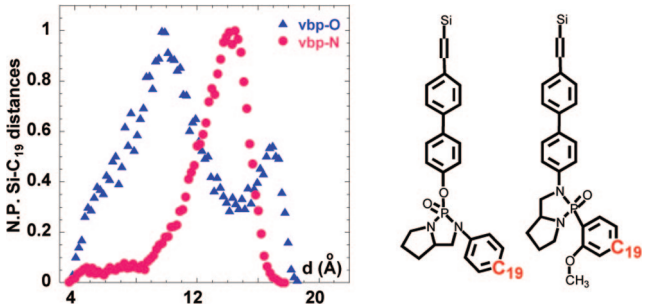

Figure 7. Distance between the Si-edge and C_{19} atoms located on the bulky groups grafted to the vbp segment as illustrated on the right-hand side.

IV.1.3. Electron Delocalization. The POSS core could be expected not to have any impact on the photophysical properties of the vbp derivatives, both because silicon has a low ability to attract electrons (Pauling electronegativity: Si 1.90)[79] and because POSS has a much larger HOMO−LUMO gap, ~6.85 eV, than vbp.[45] However, without the relative positions of the HOMO−LUMO levels no conclusion can be drawn, and consequently, the redox properties were investigated by cyclic voltammetry. In this context the electrochemical data complemented nicely the photophysical investigation completed on the free chromophore. These results also highlight a slight variation of the HOMO and LUMO levels induced by the grafted bulky groups, while the variation of the band gap determined with these two techniques was found to follow a similar trend (see Supporting Imformation for details).[76] However, in the case of the POSS derivatives, solubility issues associated with the solvents appropriate for cyclic voltammetry studies prevented a quantitative description of the energy levels of the compounds under investigation. Consequently, as solvent effects associated with cyclic voltammetry could not be completely excluded, further insight was looked for by electronic structure calculations.

The first excitation energies of the AMBER-optimized structures of the three different vbp-based chromophores were calculated (see Table 3). The hydrogen atom located on the first carbon atom of the 4-vinylbiphenyl group was then exchanged with an SiH_3 group to give an indication of the effect of the POSS core. In order to separate the electronic from the conformational effect, only the conformation of the SiH_3 group was further optimized. The simulated absorption spectra resulting from ZINDO/S calculations are displayed in Figure 4 (triangles). In all three molecules, adding an SiH_3 group leads to a small red shift of a few nanometers of the lowest energy transition (H_3Si-vbp: 321 nm; H_3Si-vbp-O: 326 nm; H_3Si-vbp-N: 333 nm), which is smaller than the shift observed experimentally, indicating only a slight increase of the conjugation length or a slight inductive effect via the delocalization of the vbp electrons to the silicon atoms. It therefore appears that the experimentally observed red shift is mainly caused by grafting the free chromophore to the POSS core of the dendritic molecules.

TABLE 3: Calculated Absorbance Peaks and Deviation When Compared to Experimental Data

structure	X-vbp	X-vbp-O	X-vbp-N
abs peak (nm) X: hydrogen	317	323	330
$\Delta_{\text{free dendrons}}$ (nm)	39	42	26
abs peak (nm) X: $-SiH_3$	322	326	333
$\Delta_{\text{dendron molecule}}$ (nm)	25	26	17
abs peak (nm) X: POSS	324	336	341
$\Delta_{\text{dendron molecule}}$ (nm)	27	36	25

The simulated absorption spectrum of the dendritic molecule with eight vbp dendrons is very similar to that of the single vbp molecule with the SiH_3 group, with only a minimal additional red shift (323 nm vs 321 nm) (see Table 3 and Figure 4 (circles)).

The dendritic molecules based on the two larger branches, POSS-vbp-O and POSS-vbp-N, show a much larger red shift of the main peak of the spectrum as well as the appearance of low-intensity peaks between 400 and 450 nm. These additional peaks observed in the calculated absorbance spectra are believed to result from interactions between two dendrons brought next to one another over the course of the annealing and minimization steps because of intramolecular interactions between bulky groups grafted to different dendron of the same dendritic molecule. These new absorption peaks are consistent and similar to those obtained via transient dipole interactions, which have been extensively studied in other systems such as coupled molecular dimers and bacteriochlorophyll chromophores in photosynthetic bacteria.[55,56] This interpretation has been confirmed by similar ZINDO/S calculations completed on fully extended conformations of the macromolecules. The spectra from these calculations are presented in the Supporting Information and do not display the low-energy extra peaks. These new peaks were not observed over the course of the present experimental study (see Figure 2) because in the experiments thermal agitation favors more open dendritic structures than the annealed and minimized conformations used for the ZINDO/S calculations shown in Figure 4. This leads to conformations between the minimized and fully extended conformations used in the two sets of ZINDO/S calculations. Indeed, intramolecular interactions between bulky groups can overcome the rigidity barrier of the vinyl bridge to the POSS core and leads the minimized structures to be more collapsed conformations so that transient dipoles on the vbp groups of the dendrons are brought within range of interacting with one another. This observation could also lead the development of a rational strategy to develop lock and key types of chemical sensors and a new class of infrared dendritic molecules for solar cell applications. This might involve bringing two dyes used to make dendrons grafted on a POSS core close to one another (via direct chemical bonding or either inter- or intramolecular interactions triggered by the bulky groups) so that interacting transient dipoles could shift the absorption spectra.

To summarize, the simulated absorption spectra of the dendritic molecules based on the two larger branches, POSS-vbp-O and POSS-vbp-N, show a larger red shift of the main peak of the spectrum than observed experimentally but succeed in reproducing the trend of the experimental data. The simulated absorption spectra also show the appearance of low-intensity peaks between 400 and 450 nm, which were not observed in our experiments. These additional peaks arise from intramolecular interactions between bulky groups on the dendrons in the optimized structures. In experimental conditions used for the photophysical characterization, the branches will be further apart due to thermal agitation.

In the context of the present work, both the cyclic voltammetry data and the electronic simulations consistently support the explanation of a slight red shift induced by a partial electron delocalization of the chromophore to the POSS core. It can be noticed that reference 86 appeared in ASAP while our work was under review suggests potential extended conjugation involving the silsesquioxane core which would agree and support our detailed analysis.

IV.2. PLQY/Lifetime Variations. The most striking result we report on is the opposite variations of both PLQY and PL liftetime between free dendrons and dendritic molecules when bulky groups are grafted to the chromophores. Energy transfer was not observed for any of the compounds under investigation. Time-resolved PL measurements showed that the monoexponential decay in vbp was altered by the grafting, suggesting that the species accessed several conformations, all contributing to the relaxation process. The PL efficiency and lifetimes also appear to be strongly altered by both the grafted bulky groups and the chromophores' confinement around the 0.53 nm POSS core. In the first case, the PL efficiency and the average lifetimes fall drastically from vbp to vbp-N (see Table 1). In the latter case, the PLQY and the lifetimes increase (see Table 1) with those for POSS-vbp-N, reaching even higher values than those obtained with the free unaltered vbp chromophores. This behavior and apparently opposed trends are, however, consistent with a framework based on tuning the access of the vbp groups to nonradiative relaxation pathways. These relaxation pathways competing with the emission of photons as the chromophore relaxes to its ground state include (a) electronic perturbations and quenching by charge transfer and excimer formation, (b) isomerization, and (c) rigidochromism via the variation of the accessible degree of freedom (vibrational, translational, rotational).

IV.2.1. Electronic Perturbation/Charge Transfer and Excimer Formation. When comparing vbp, vbp-O, and vbp-N chromophores, cyclic voltammetry data suggest a first reduction peak variation (see Supporting Information for details), which indicates a weak alteration of the ability of the molecules to gain electrons (vbp > vbp-N > vbp-O). This implies that the phenyl ring located on the bulky group (see Figure 1) does not favor charge transfer away from the vbp.

In the case of the POSS derivatives, as all the dendrons are identical, there is nothing to drive any intramolecular charge transfer from one dendron to another.

Emission of excimers is usually strongly red-shifted, structureless, and long-lived. Intramolecular excimer could be conceived as two chromophores, at least one of which would be in an electronic excited state, on the same dendritic molecules and close enough to interact and form a short-lived dimeric aggregate. Even though for all the compounds the emission spectra and the energy width transitions are red-shifted and larger than those of the free vbp chromophore, only vbp-O shows a lifetime component longer than vbp, 2.39 vs 1.58 ns (see Table 1). Consequently, a weak charge transfer cannot be completely ruled out; however, no evidence of such charge transfer was provided experimentally, so that other relaxation paths should be considered to be more likely.

IV.2.2. E−Z Isomers (NMR-MD). As presented in Table 1, POSS-vbp shows a very low PLQY (4%), while the PLQY of POSS-vbp-O and POSS-vbp-N increases to 14 and 58%, respectively. At first sight, this could be interpreted as *cis−trans* isomerization being prevented by the bulky group connected to the terminal position of the vbp. Indeed, it is a well-known fact in photophysics that when a system can readily undergo *cis−trans* isomerization, this usually leads to low emission quantum yields.

However, photoisomerization can be excluded as a major contribution to our experimental results, as none of the ^{1}H NMR spectra of the dendritic molecules show any trace of contamination. All of the double bonds have *E* configuration ($J_{HH} \approx 19$ Hz) so that intrinsic *E−Z* isomerization can be ruled out (see Supporting Information for details).[76] Photoisomerization was

tested by changing the exposure time to excitation wavelengths at 5 kHz which did not induce any variation of the photophysical properties reported herein, excluding the formation of long-lived isomers.

IV.2.3. Degree of Freedom vs Confinement. It is well established that increasing the degrees of freedom (vibrational, translational, rotational) of a dye very often leads to a variation of its PLQY. This phenomenon has been demonstrated by both changing the solvent viscosity (by using different solvents, a single solvent at various pressures, or solid solutions) and adding bulky groups of different sizes to different dyes so that torsional, rotational, and vibrational degrees of freedom were altered in a similar way as rigidochromism has been reported in some organic dyes sytems.[87−89] In this context, it can be considered that, by grafting bulky groups to vpb, the resulting chromophores have access to more degrees of freedom (rotations, conformations, and vibrations), offering additional relaxation paths, which compete efficiently with the radiative relaxation and lead to lower PLQY. This argument can also be used while comparing free vbp with POSS-vbp (45 vs 4%, a decrease of more than 1 order of magnitude) and vbp-O with POSS-vbp-O (38 vs 14%, differing by only a factor 2.7) (see Table 1). This is supported by molecular dynamics simulations, which show free rotation of the vbp around the $Si-C_1$ axes in the case of POSS-vbp whereas this free rotation about the both $Si-C_1$ axes is hindered by the bulky groups in the cases of both POSS-vbp-O and POSS-vbp-N. Consequently, it is consistent for POSS-vbp to have a much lower PLQY than both POSS-vbp-O and POSS-vbp-N.

The backfolding revealed by the molecular dynamics simulations can then be used to gain insight about the PLQYs of the more complexe dendritic molecules. Figure 7 indicates that the inner spaces between the branches allow partial back folding of grafted external groups. This also suggests that POSS-vbp-O adopts two main conformations (with $Si-C_{19}$ peaks at 9.9 and 17 Å), consistent with the multi-exponential decay of the time-resolved fluorescence reported in Table 1 as well as with the flexibility of the oxygen bridge. In contrast, POSS-vbp-N shows only a single main conformation (with a $Si-C_{19}$ peak at 14.1 Å), consistent with the large amplitude, 0.78, of its long-lived component with a lifetime of 1.53 ns.

The modeling provides dynamic pictures of the conformations accessible to the dendritic molecules. Because backfolded and extended as well as conformations all the intermediates can be seen in Figure 7, the broadness and peak ratios of the $Si-C_{19}$ distance population are indicative of the mobility of the branches. The population distributions illustrate how many conformations are accessible to the macromolecules. Intramolecular and solvent interactions, entropy, and thermal agitation determine whether or not these conformations will in fact be accessed, but the assessment of these properties is beyond the scope of our work. In the case of POSS-vbp-N, molecular dynamics calculations show that backfolding is considerably reduced with a single main $Si-C_{19}$ peak at ~14.1 Å only tailing off at shorter distances (see Figure 7). This is consistent with both a bulkier group (terminal $-OCHH_3$ group) and the nitrogen ring lock used as a bridge (see Figure 1). This rigid nitrogen ring lock further reduces the number of degrees of freedom accessible to the branches grafted to the POSS core and explains why the PLQY of this dendritic molecule is much larger than that of its free chromophore, 58 vs 4%, even larger than the free vbp chromophore (see Table 1).

As explained earlier, both POSS-vbp-O and POSS-vbp-N have reduced opportunities of rotation around $Si-C_1$ axes when compared to POSS-vbp and hence higher PLQYs. However, the arguments discussed above suggest that POSS-vbp-N displays a reduced mobility of its external bulky group when compared to POSS-vbp-O (see Figure 7), consistent with a larger PLQY.

The picture we have presented is also capable of explaining the luminescence of pyrene-functionalized POSS core dendritic molecules, which in the context of the organic light-emitting diodes, have been shown to be highly emissive as opposed to most of pyrene-based materials that are nonemissive in the solid state.[52] In the pyrene POSS derivatives a red shift and an increase of the solution PL efficiency were reported. Detailed molecular dynamics simulations of the pyrene POSS family of dendritic molecules investigated by Lo et al. have also been completed over the course of our work, supporting both the interpretation and strategy we have described with our family of new dendritic molecules.

Our investigation suggests that steric hindrance and confinement as well as intramolecular interactions between the pyrene branches reduce the range of accessible conformations and sterically prevent rotation around the chemical bond to the POSS core. The pyrene and vbp derivatives have been synthesized via different chemical paths, either cross-metathesis or Heck conditions, and in both cases the reduction of intramolecular degrees of freedom resulted in a higher solution PLQY. This supports the generality of our results while re-emphasizing the large potential offered by dendritic molecules based on a POSS core for the design of efficient photoluminescent materials for organic light-emitting diodes.

V. Conclusion

Steady-state and time-resolved spectroscopy along with molecular dynamics and electronic structure techniques have been used to gain insight into the photophysical properties of hybrid dendritic molecules. A silsesquioxane cube was used as the core and was shown to only weakly alter the photophysical properties of the chemically bonded chromophores. However, addition of bulky groups by rigid bridges to the branches, providing increased steric hindrance, has successfully reduced the number of intramolecular degrees of freedom, which in turn has favored radiative relaxation and provided a trigger to alter the PL efficiency of silsesquioxane-based dendritic molecules.

The apparent contrast between free chromophores and dendritic molecules is the key element of this work, and this leads to a general strategy for tuning the photoluminescence efficiency of dendritic molecules by selecting appropriate bulky groups providing different degrees of effective dendron steric hindrance as well as by choosing an appropriate chemical bridge connecting the chromophores and bulky groups. The POSS-based dendritic molecule can then be tailored not only by changing the chromophore but also by altering the dendritic molecule generation and/or the bridged group to provide steric interactions and allow a fine-tuning of the photophysical properties. This is of considerable importance in the design of dendritic light-emitting materials.

Acknowledgment. The authors gratefully acknowledge the Royal Society for the provision of a K. C. Wong Fellowship (G.C.) as well as the Engineering and Physical Sciences Research Council (EPSRC, P.A., G.C.) and the Scottish Higher Education Funding Council (SHEFC) for financial support. P.A. gratefully acknowledges the Scottish Universities Physics Alliance for funding of his SUPA Advanced Research Fellowship. P.A. also thanks Katherine Haxton for stimulating initial

molecular dynamic related discussions as well as Frédérique Menu and Aly Gillies while developing the C++ data analysis code. T.v.M. gratefully acknowledges the Royal Society for its support under the University Research Fellowship scheme. We thank EaStCHEM for computational support via the EaStCHEM Research Computing Facility.

Supporting Information Available: Experimental characterization of the compounds; details of cyclic voltammetry, optical spectroscopy, simulations, and molecular dynamics. This material is available free of charge via the Internet at http://pubs.acs.org.

References and Notes

(1) Hecht, S.; Frechet, J. M. J. *Angew. Chem., Int. Ed.* **2001**, *40* (1), 74–91.
(2) Momotake, A.; Arai, T. *Polymer* **2004**, *45* (16), 5369–5390.
(3) Miller, L. L.; Duan, R. G.; Tully, D. C.; Tomalia, D. A. *J. Am. Chem. Soc.* **1997**, *119* (5), 1005–1010.
(4) Schalley, C. A.; Vögtle, F. *Dendrimers V: Functional and Hyperbranched Building Blocks, Photophysical Properties, Applications in Materials and Life Sciences*; Springer-Verlag: Berlin, 2003.
(5) Ropartz, L.; Morris, R. E.; Foster, D. F.; Cole-Hamilton, D. J. *Chem. Commun.* **2001**, (4), 361–362.
(6) Twyman, L. J.; King, A. S. H.; Martin, I. K. *Chem. Soc. Rev.* **2002**, *31* (2), 69–82.
(7) Ropartz, L.; Haxton, K. J.; Foster, D. F.; Morris, R. E.; Slawin, A. M. Z.; Cole-Hamilton, D. J. *J. Chem. Soc., Dalton Trans.* **2002**, (23), 4323–4334.
(8) Liang, C.; Frechet, J. M. J. *Prog. Polym. Sci.* **2005**, *30* (3−4), 385–402.
(9) Flomenbom, O.; Amir, R. J.; Shabat, D.; Klafter, J. *J. Lumin.* **2005**, *111* (4), 315–325.
(10) Khopade, A. J.; Caruso, F. *Biomacromolecules* **2002**, *3* (6), 1154–1162.
(11) Furuta, P.; Frechet, J. M. J. *J. Am. Chem. Soc.* **2003**, *125* (43), 13173–13181.
(12) Goetheer, E. L. V.; Baars, M.; van den Broeke, L. J. P.; Meijer, E. W.; Keurentjes, J. T. F. *Ind. Eng. Chem. Res.* **2000**, *39* (12), 4634–4640.
(13) Chen, G. H.; Guan, Z. B. *J. Am. Chem. Soc.* **2004**, *126* (9), 2662–2663.
(14) Cornelissen, J. J. L. M.; van Heerbeek, R.; Kamer, P. C. J.; Reek, J. N. H.; Sommerdijk, N. A. J. M.; Nolte, R. J. M. *Adv. Mater.* **2002**, *14* (7), 489−492.
(15) Yeung, L. K.; Crooks, R. M. *Nano Lett.* **2001**, *1* (1), 14–17.
(16) Burn, P. L.; Lo, S. C.; Samuel, I. D. W. *Adv. Mater.* **2007**, *19* (13), 1675–1688.
(17) Balzani, V.; Ceroni, P.; Juris, A.; Venturi, M.; Campagna, S.; Puntoriero, F.; Serroni, S. *Coord. Chem. Rev.* **2001**, *219*, 545–572.
(18) Ceroni, P.; Bergamini, G.; Marchioni, F.; Balzani, V. *Prog. Polym. Sci.* **2005**, *30* (3−4), 453–473.
(19) Halim, M.; Pillow, J. N. G.; Samuel, D. W.; Burn, P. L. *Adv. Mater.* **1999**, *11* (5), 371–374.
(20) Weil, T.; Reuther, E.; Müllen, K. *Angew. Chem., Int. Ed.* **2002**, *41* (11), 1900–1904.
(21) Goodson, T.; Varnavski, O.; Wang, Y. *Int. Rev. Phys. Chem.* **2004**, *23* (1), 109–150.
(22) Pillow, J. N. G.; Halim, M.; Lupton, J. M.; Burn, P. L.; Samuel, I. D. W. *Macromolecules* **1999**, *32* (19), 5985–5993.
(23) Lupton, J. M.; Samuel, I. D. W.; Beavington, R.; Burn, P. L.; Bassler, H. *Adv. Mater.* **2001**, *13* (4), 258–261.
(24) Frampton, M. J.; Namdas, E. B.; Lo, S.-C.; Burn, P. L.; Samuel, I. D. W. *J. Mater. Chem.* **2004**, *14* (19), 2881−2888.
(25) Markham, J. P. J.; Namdas, E. B.; Anthopoulos, T. D.; Samuel, I. D. W.; Richards, G. J.; Burn, P. L. *Appl. Phys. Lett.* **2004**, *85* (9), 1463–1465.
(26) Kwon, T. W.; Alam, M. M.; Jenekhe, S. A. *Chem. Mat.* **2004**, *23* (16), 4657−4666.
(27) Lo, S. C.; Male, N. A. H.; Markham, J. P. J.; Magennis, S. W.; Burn, P. L.; Salata, O. V.; Samuel, I. D. W. *Adv. Mater.* **2002**, *14* (13−14), 975–979.
(28) Liu, D. J.; De Feyter, S.; Cotlet, M.; Stefan, A.; Wiesler, U. M.; Herrmann, A.; Grebel-Koehler, D.; Qu, J. Q.; Müllen, K.; De Schryver, F. C. *Macromolecules* **2003**, *36* (16), 5918–5925.
(29) Huang, B. H.; Prantil, M. A.; Gustafson, T. L.; Parquette, J. R. *J. Am. Chem. Soc.* **2003**, *125* (47), 14518–14530.
(30) Wang, B. B.; Zhang, X.; Jia, X. R.; Li, Z. C.; Ji, Y.; Yang, L.; Wei, Y. *J. Am. Chem. Soc.* **2004**, *126* (46), 15180–15194.
(31) Swallen, S. F.; Zhu, Z. G.; Moore, J. S.; Kopelman, R. *J. Phys. Chem. B* **2000**, *104* (16), 3988–3995.
(32) Baker, L. A.; Crooks, R. M. *Macromolecules* **2000**, *33* (24), 9034–9039.
(33) Tomalia, D. A. *Prog. Polym. Sci.* **2005**, *30* (3−4), 294–324.
(34) Lor, M.; Jordens, S.; De Belder, G.; Schweitzer, G.; Fron, E.; Viaene, L.; Cotlet, M.; Weil, T.; Mullen, K.; Verhoeven, J. N.; Van der Auweraer, M.; De Schryver, F. C. *Photochem. Photobiol. Sci.* **2003**, *2* (5), 501–510.
(35) Schweitzer, G.; Gronheid, R.; Jordens, S.; Lor, M.; De Belder, G.; Weil, T.; Reuther, E.; Mullen, M.; De Schryver, F. C. *J. Phys. Chem. A* **2003**, *107* (18), 3199–3207.
(36) Cotlet, M.; Gronheid, R.; Habuchi, S.; Stefan, A.; Barbafina, A.; Müllen, K.; Hofkens, J.; De Schryver, F. C. *J. Am. Chem. Soc.* **2003**, *125* (44), 13609–13617.
(37) De Schryver, F. C.; Vosch, T.; Cotlet, M.; Van der Auweraer, M.; Mullen, K.; Hofkens, J. *Acc. Chem. Res.* **2005**, *38* (7), 514–522.
(38) Vosch, T.; Cotlet, M.; Hofkens, J.; Van der Biest, K.; Lor, M.; Weston, K.; Tinnefeld, P.; Sauer, M.; Latterini, L.; Mullen, K.; De Schryver, F. C. *J. Phys. Chem. A* **2003**, *107* (36), 6920–6931.
(39) Maus, M.; Mitra, S.; Lor, M.; Hofkens, J.; Weil, T.; Herrmann, A.; Mullen, K.; De Schryver, F. C. *J. Phys. Chem. A* **2001**, *105* (16), 3961–3966.
(40) Oesterling, I.; Mullen, K. *J. Am. Chem. Soc.* **2007**, *129* (15), 4595–4605.
(41) Karni, Y.; Jordens, S.; De Belder, G.; Schweitzer, G.; Hofkens, J.; Gensch, T.; Maus, M.; De Schryver, F. C.; Hermann, A.; Mullen, K. *Chem. Phys. Lett.* **1999**, *310* (1−2), 73–78.
(42) Pina, F.; Passaniti, P.; Maestri, M.; Balzani, V.; Vögtle, F.; Gorka, M.; Lee, S.-K.; van Heyst, J.; Fakhrnabavi, H. *ChemPhysChem* **2004**, *5* (4), 473–480.
(43) Tsuda, K.; Dol, G. C.; Gensch, T.; Hofkens, J.; Latterini, L.; Weener, J. W.; Meijer, E. W.; De Schryver, F. C. *J. Am. Chem. Soc.* **2000**, *122* (14), 3445–3452.
(44) Jaffres, P. A.; Morris, R. E. *J. Chem. Soc., Dalton Trans.* **1998**, (16), 2767–2770.
(45) Lin, T. T.; He, C. B.; Xiao, Y. *J. Phys. Chem. B* **2003**, *107* (50), 13788–13792, and references therein.
(46) Brick, C. M.; Ouchi, Y.; Chujo, Y.; Laine, R. M. *Macromolecules* **2005**, *38* (11), 4661–4665.
(47) Choi, J.; Harcup, J.; Yee, A. F.; Zhu, Q.; Laine, R. M. *J. Am. Chem. Soc.* **2001**, *123* (46), 11420–11430.
(48) Baker, E. S.; Gidden, J.; Anderson, S. E.; Haddad, T. S.; Bowers, M. T. *Nano Lett.* **2004**, *4* (5), 779–785.
(49) Xiao, S.; Nguyen, M.; Gong, X.; Cao, Y.; Wu, H. B.; Moses, D.; Heeger, A. J. *Adv. Funct. Mater.* **2003**, *13* (1), 25–29.
(50) Lin, W. J.; Chen, W. C.; Wu, W. C.; Niu, Y. H.; Jen, A. K. Y. *Macromolecules* **2004**, *37* (7), 2335–2341.
(51) Lo, M. Y.; Ueno, K.; Tanabe, H.; Sellinger, A. *Chem. Rec.* **2006**, *6* (3), 157–168.
(52) Lo, M. Y.; Zhen, C.; Lauters, M.; Jabbour, G. E.; Sellinger, A. *J. Am. Chem. Soc.* **2007**, *129* (18), 5808–5809.
(53) Sellinger, A.; Tamaki, R.; Laine, R. M.; Ueno, K.; Tanabe, H.; Williams, E.; Jabbour, G. E. *Chem. Commun.* **2005**, (29), 3700–3702.
(54) Froehlich, J. D.; Young, R.; Nakamura, T.; Ohmori, Y.; Li, S.; Mochizuki, A.; Lauters, M.; Jabbour, G. E. *Chem. Mater.* **2007**, *19* (20), 4991–4997.
(55) Scholes, G. D.; Gould, I. R.; Cogdell, R. J.; Fleming, G. R. *J. Phys. Chem. B* **1999**, *103* (13), 2543–2553.
(56) Myers Kelley, A. *J. Chem. Phys.* **2003**, *119* (6), 3320–3331.
(57) Beenken, W. J. D.; Lischka, H. *J. Chem. Phys.* **2005**, *123* (14), 144311.
(58) Cavallo, L.; Fraternali, F. *Chem.—Eur. J.* **1998**, *4* (5), 927–934.
(59) Gorman, C. B.; Smith, J. C. *Polymer* **2000**, *41* (2), 675–683.
(60) Scherrenberg, R.; Coussens, B.; van Vliet, P.; Edouard, G.; Brackman, J.; de Brabander, E.; Mortensen, K. *Macromolecules* **1998**, *31* (2), 456–461.
(61) Zacharopoulos, N.; Economou, L. G. *Macromolecules* **2002**, *35* (5), 1814–1821.
(62) Haxton, K. J.; Cole-Hamilton, D. J.; Morris, R. E. *Dalton Trans.* **2004**, (11), 1665–1669.
(63) Lamm, M. H.; Chen, T.; Glotzer, S. C. *Nano Lett.* **2003**, *3* (8), 989–994.
(64) Berlman, I. B. *Handbook of Fluorescence Spectra of Aromatic Molecules*; Academic Press: New York, 1971.
(65) Hunter, C. A.; Lawson, K. R.; Perkins, J.; Urch, C. J. *J. Chem. Soc., Perkin Trans. 2* **2001**, (5), 651–669.
(66) Cheng, G.; André, P.; Vautravers, N.; Samuel, I. D. W.; Cole-Hamilton, D. Manuscript in preparation.
(67) Demas, J. N.; Crosby, G. A. *J. Phys. Chem.* **1971**, *75* (8), 991−1024.
(68) Lakowicz, J. R. *Principles of Fluorescence Spectroscopy*, 2nd ed.; Plenum: New York, 1999.

(69) Pommerehne, J.; Vestweber, H.; Guss, W.; Mahrt, R. F.; Bassler, H.; Porsch, M.; Daub, J. *Adv. Mater.* **1995**, *7* (6), 551–554.

(70) Micaroni, L.; Nart, F. C.; Hummelgen, I. A. *J. Solid State Electrochem.* **2002**, *7* (1), 55–59.

(71) Becke, A. D. *J. Chem. Phys.* **1993**, *98* (7), 5648–5652.

(72) Bauernschmitt, R.; Ahlrichs, R. *Chem. Phys. Lett.* **1996**, *256* (4−5), 454–464.

(73) Head-Gordon, M.; Rico, R. J.; Oumi, M.; Lee, T. J. *Chem. Phys. Lett.* **1994**, *219* (1−2), 21–29.

(74) Head-Gordon, M.; Maurice, D.; Oumi, M. *Chem. Phys. Lett.* **1995**, *246* (1−2), 114–121.

(75) Ridley, J.; Zerner, M. *Theor. Chim. Acta* **1973**, *32* (2), 111–134.

(76) Neese, F. ORCA: An ab Initio, DFT and Semiempirical Electronic Structure Package 2.6 (Revision 00), 2007.

(77) Frisch, M. J.; Trucks, G. W.; Schlegel, H. B.; Scuseria, G. E.; Robb, M. A.; Cheeseman, J. R.; Montgomery, J.; J. A., Vreven, T.; Kudin, K. N.; Burant, J. C.; Millam, J. M.; Iyengar, S. S.; Tomasi, J.; Barone, V.; Mennucci, B.; Cossi, M.; Scalmani, G.; Rega, N.; Petersson, G. A.; Nakatsuji, H.; Hada, M.; Ehara, M.; Toyota, K.; Fukuda, R.; Hasegawa, J.; Ishida, M.; Nakajima, T.; Honda, Y.; Kitao, O.; Nakai, H.; Klene, M.; Li, X.; Knox, J. E.; Hratchian, H. P.; Cross, J. B.; Bakken, V.; Adamo, C.; Jaramillo, J.; Gomperts, R.; Stratmann, R. E.; Yazyev, O.; Austin, A. J.; Cammi, R.; Pomelli, C.; Ochterski, J. W.; Ayala, P. Y.; Morokuma, K.; Voth, G. A.; Salvador, P.; Dannenberg, J. J.; Zakrzewski, V. G.; Dapprich, S.; Daniels, A. D.; Strain, M. C.; Farkas, O.; Malick, D. K.; Rabuck, A. D.; Raghavachari, K.; Foresman, J. B.; Ortiz, J. V.; Cui, Q.; Baboul, A. G.; Clifford, S.; Cioslowski, J.; Stefanov, B. B.; Liu, G.; Liashenko, A.; Piskorz, P.; Komaromi, I.; Martin, R. L.; Fox, D. J.; Keith, T.; Al-Laham, M. A.; Peng, C. Y.; Nanayakkara, A.; Challacombe, M.; Gill, P. M. W.; Johnson, B.; Chen, W.; Wong, M. W.; Gonzalez, C.; Pople, J. A. Gaussian 03 (Revision C.02), 2004.

(78) Hyperchem.

(79) Lide, D. R.; Weast, R. C.; Company, C. R. *CRC Handbook of Chemistry and Physics*; CRC Press: Boca Raton, FL, 2002.

(80) Arulmozhiraja, S.; Fujii, T. *J. Chem. Phys.* **2001**, *115* (23), 10589–10594.

(81) Almenningen, A.; Bastiansen, O.; Fernholt, L.; Cyvin, B. N.; Cyvin, S. J.; Samdal, S. *J. Mol. Struct.* **1985**, *128* (1−3), 59–76.

(82) Tsuzuki, S.; Uchimaru, T.; Matsumura, K.; Mikami, M.; Tanabe, K. *J. Chem. Phys.* **1999**, *110* (6), 2858–2861.

(83) Grein, F. *J. Mol. Struct. (THEOCHEM)* **2003**, *624*, 23–28.

(84) Pope, M. Swenberg, C. E., *Electronic Processes in Organic Crystals and Polymers*; Oxford University Press: New York, 1999.

(85) Kohn, F.; Hofkens, J.; Wiesler, U. M.; Cotlet, M.; van der Auweraer, M.; Mullen, K.; De Schryver, F. C. *Chem.—Eur. J.* **2001**, *7* (19), 4126–4133.

(86) Sulaiman, S.; Bhaskar, A.; Zhang, J.; Guda, R.; Goodson, T., III; Laine, R. M. *Chem. Mater.* **2008**, ASAP Article (DOI: 10.1021/cm801017e). While our manuscript was under review the Grubbs method for the synthesis of POSS derivatives and related molecules has been reported by Laine's group, with photophysical characterization also suggesting potential extended conjugation involving the silsesquioxane core.

(87) Van der Auweraer, M.; Van den Zegel, M.; Boens, N.; Deschryver, F. C.; Willig, F. *J. Phys. Chem.* **1986**, *90* (6), 1169–1175.

(88) Sauerwein, B.; Murphy, S.; Schuster, G. B. *J. Am. Chem. Soc.* **1992**, *114* (20), 7920–7922.

(89) Murphy, S.; Schuster, G. B. *J. Phys. Chem.* **1995**, *99* (21), 8516–8518.

JP806031Q